Supporting Information

Rhee et al. 10.1073/pnas.1411932111

SI Text

SI Materials and Methods

Linear Noise Decomposition. Here, we derive the noise decomposition equations shown in Eqs. **4–6** in the main text, under the assumptions described therein. We begin by examining the top portion of the four-node motif shown in Fig. 1*C* where a discrete signal S is transmitted to an intermediary node L. The intermediary L can then be described as a function of the signal S and a stochastic noise term η_L, defined as the trunk noise:

$$L = f(S) + \eta_L. \tag{S1}$$

Downstream, the signal bifurcates along two separate pathways to the readouts X and Y. Because X and Y are both affected by L, they can be represented as distinct linear functions of L (or of some transformation of L) plus a corresponding stochastic noise term η_X or η_Y, defined as the branch noise. This is represented as follows, where m and b are the linear coefficients:

$$\begin{aligned} X &= m_X \cdot L + b_X + \eta_X \\ Y &= m_Y \cdot L + b_Y + \eta_Y. \end{aligned} \tag{S2}$$

We assume the above noise terms are independent, additive, and have zero mean. By taking the variance of Eq. **S1**, we find that the magnitude of the trunk noise is equal to $var(L)$. Because the noise terms are independent, they have zero pairwise covariance; thus, by taking the covariance of X and Y and rearranging we obtain

$$\frac{cov(X,Y)}{m_X m_Y} = var(L) = \sigma^2_{\eta_L}.$$

This choice defines the trunk noise in the units of L, whereas dividing or multiplying by r, as defined below, can convert the trunk noise into units of X or Y, respectively. Furthermore, by taking the variance of Eq. **S2** we obtain

$$\begin{aligned} var(X) &= m_X^2 \cdot var(L) + \sigma^2_{\eta_X} \\ var(Y) &= m_Y^2 \cdot var(L) + \sigma^2_{\eta_Y}, \end{aligned} \tag{S3}$$

where the branch noise terms $\sigma^2_{\eta_X}$ and $\sigma^2_{\eta_Y}$ denote the variance of η_X and η_Y. We can therefore see that

$$\sigma^2_{\eta_L} = cov(X,Y), \tag{S4}$$

$$\sigma^2_{\eta_X} = var(X) - \frac{\sigma^2_{\eta_L}}{r}, \tag{S5}$$

$$\sigma^2_{\eta_Y} = var(Y) - r \cdot \sigma^2_{\eta_L}, \tag{S6}$$

where $r = m_Y/m_X$. Importantly, r is the slope of the line of Y versus X in the absence of noise. This line is parameterized directly by L and indirectly by S. Thus, the line can be obtained by calculating the regression of the average of Y versus the average of X at various levels of S, allowing r to be experimentally estimated (Fig. S3). Because the variances of X and Y and their covariance are experimentally measurable, Eqs. **S4–S6** allow for direct estimation of the branch and trunk noises.

Relation to the Methods of Elowitz et al. and Swain et al. In this section, we will demonstrate that the trunk–branch decomposition is a more generalized formulation of the methods pioneered by Elowitz et al. (1) and Swain et al. (2). To begin, we note the nonnormalized definitions of the intrinsic and extrinsic noise:

$$\eta^2_{int} = \frac{1}{2}\left\langle (X-Y)^2 \right\rangle; \quad \eta^2_{ext} = \langle XY \rangle - \langle X \rangle \langle Y \rangle. \tag{S7}$$

From this definition, we can immediately see that the extrinsic noise is equivalent to the previously defined trunk noise (Eq. **S4**). In the case of equivalent dual reporters, X and Y are statistically equivalent, hence $\langle X \rangle = \langle Y \rangle$ and $r = 1$. By taking advantage of these properties, we can then enumerate several parallels between the trunk–branch and the intrinsic–extrinsic methodologies.

Similarly, we note that the intrinsic noise is equivalent to the average of the branch noises from Eqs. **S5** and **S6**, proven as follows:

$$\begin{aligned} \frac{1}{2}\left(\sigma^2_{\eta_X} + \sigma^2_{\eta_Y}\right) &= \frac{1}{2}\left(var(X) + var(Y) - 2cov(X,Y)\right) \\ &= \frac{1}{2}\left(\langle X^2 \rangle - \langle X \rangle^2 + \langle Y^2 \rangle - \langle Y \rangle^2 - 2\langle XY \rangle + 2\langle X \rangle \langle Y \rangle\right) \\ &= \frac{1}{2}\left(\langle X^2 \rangle + \langle Y^2 \rangle - 2\langle XY \rangle\right) \\ &= \frac{1}{2}\left\langle (X-Y)^2 \right\rangle. \end{aligned} \tag{S8}$$

Using the above relationships, we can also easily prove statements made in the main text about extrinsic and intrinsic noise. First, using Eq. **S8**, we can show that intrinsic noise is proportional to the variance of the difference in reporter expression:

$$\begin{aligned} \frac{1}{2}\left\langle (X-Y)^2 \right\rangle &= \frac{1}{2}\left(var(X) + var(Y) - 2cov(X,Y)\right) \\ &= \frac{1}{2} var(X-Y). \end{aligned} \tag{S9}$$

Lastly, because total noise is defined as the sum of the intrinsic and extrinsic noise values, we sum the contributions and find that the total noise can be rewritten as the average variance of the reporters:

$$\begin{aligned} \sigma^2_{tot} = \sigma^2_{int} + \sigma^2_{ext} &= \frac{1}{2}\left(\sigma^2_{\eta_X} + \sigma^2_{\eta_Y}\right) + cov(X,Y) \\ &= \frac{1}{2}\left(var(X) + var(Y)\right). \end{aligned} \tag{S10}$$

Numerical Estimation of Branch and Trunk Noise. We observe that at low expression levels, our noise decomposition methodology may give unreliable estimates. This is likely due to experimental noise overwhelming the true signal when the target protein expression level is low or absent. Therefore, to estimate the percent branch or trunk noise for a given pathway, we calculate the percent branch or trunk noise for all TNF concentrations at which the protein of interest is fully expressed (≥ 0.9 ng/mL) (Fig. 3 *B–D*) and then average these calculations to arrive at a final estimate for the pathway.

We also note that due to the sensitive nature of covariances and variances to experimental error, the noise decomposition will occasionally yield slightly negative noise for branches that contribute relatively little noise to the total variability. In such cases, we interpret the results to indicate negligible noise rather than a reduction of the total amount of noise.

Noise Decomposition of Larger Networks. To decompose a larger system such as the six-node TNF–NF-κB–JNK network (Fig. 3*A*), we first note that it has three embedded four-node motifs (Fig. 3 *B–D*). By decomposing each motif, we find that although we can obtain a single noise estimate for each segment of the larger network, for one segment of the network we obtain two redundant estimates. For this particular segment, we average these two estimates to obtain a final estimate.

For example, by decomposing the noise in the NF-κB/p-c-Jun pairing, we find that 76% of the noise in p-c-Jun can be ascribed to the TNFR to p-c-Jun segment, whereas the remaining 24% is due to noise at the TNF–TNFR level. In a similar fashion, from the p-ATF-2/p-c-Jun pair, we find that 62% of the noise in p-c-Jun can be ascribed to the JNK to p-c-Jun segment. Thus, the signaling segment connecting TNFR to JNK must contribute $76\% - 62\% = 14\%$ to the variance in p-c-Jun. To assign relative noise contributions for each part of the TNF signaling network, as described in the main text, we normalize all values to the TNF to TNFR segment. Thus, the TNF to TNFR segment becomes 1, the JNK to p-c-Jun segment becomes $62\%/24\% \sim 2.6$, and we arrive with a normalized estimate of $14\%/24\% \sim 0.6$ for the TNFR to JNK segment. We conduct the same analysis by using the noise decomposition from the NF-κB/p-ATF-2 and p-ATF-2/p-c-Jun pairings and arrive at an estimate of 1.2 for the TNFR to JNK segment. We then average the two figures to arrive at a final noise estimate of 0.9 for the TNFR to JNK segment (Fig. 4*A*).

Finally, we note that to properly measure true biological noise in cellular signaling systems, the experimental error needs to be quantified and removed from the total measured variability. In our previous work, using the correlation between direct GFP fluorescence and the indirect anti-GFP immunofluorescent signal, we estimated that immunostaining accounts for less than ~12% of the measured variance in the anti-GFP signal (3).

To further validate this estimate, we obtained p65-knockout mouse embryonic fibroblast cells that were reconstituted with a p65-GFP fusion protein (4). The cells were stimulated with a range of TNF concentrations, fixed, and then immunostained. We observed a strong linear correlation between the direct and stained p65 measurements and on average $\rho \sim 0.94$ (Fig. S2).

Furthermore, as previously shown (3), if we assume that the immunostained p65 measurement is proportional to the p65 concentration and all distributions are Gaussian, we can estimate that $1 - 0.94^2 \sim 12\%$ of the observed variance is contributed by experimental noise which is similar to estimates made in previous reports (3, 5). Therefore, to correct for the experimental noise, we reduced all variances by 12%. We find that this does not significantly alter any conclusions.

1. Elowitz MB, Levine AJ, Siggia ED, Swain PS (2002) Stochastic gene expression in a single cell. *Science* 297(5584):1183–1186.
2. Swain PS, Elowitz MB, Siggia ED (2002) Intrinsic and extrinsic contributions to stochasticity in gene expression. *Proc Natl Acad Sci USA* 99(20):12795–12800.
3. Cheong R, Rhee A, Wang CJ, Nemenman I, Levchenko A (2011) Information transduction capacity of noisy biochemical signaling networks. *Science* 334(6054):354–358.
4. Lee TK, et al. (2009) A noisy paracrine signal determines the cellular NF-kappaB response to lipopolysaccharide. *Sci Signal* 2(93):ra65.
5. Dubuis JO, Samanta R, Gregor T (2013) Accurate measurements of dynamics and reproducibility in small genetic networks. *Mol Syst Biol* 9:639.

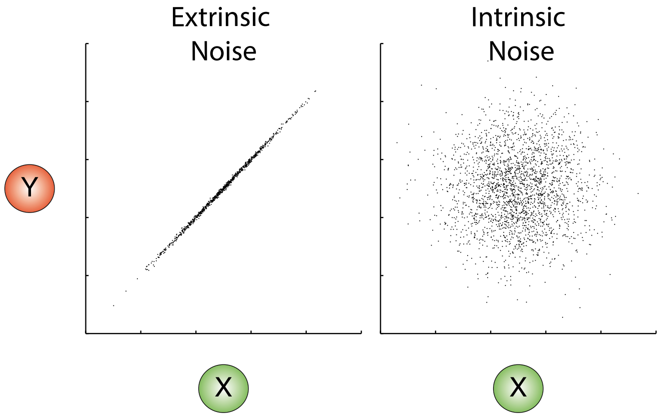

Fig. S1. Isotropic interpretation of extrinsic and intrinsic noise. Simulated data for the reporters given in Fig. 1*A* separated into extrinsic and intrinsic noise contributions. Under the assumption that the reporters do not feedback upon their regulators (1), extrinsic noise will cause a dispersion of points along the line $Y = X$, whereas intrinsic noise will contribute uncorrelated noise.

1. Stamatakis M, Adams RM, Balázsi G (2011) A common repressor pool results in indeterminacy of extrinsic noise. *Chaos* 21(4):047523.

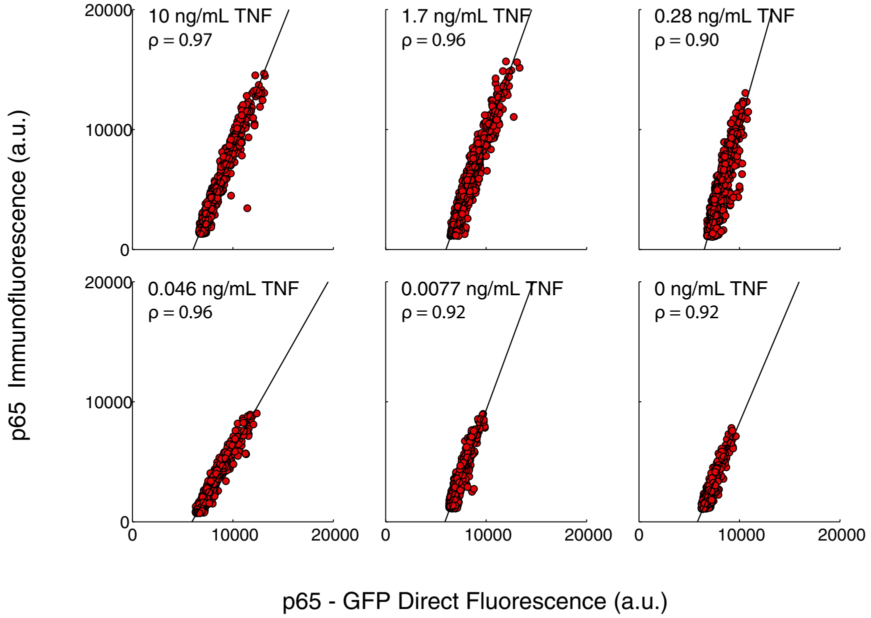

Fig. S2. Experimental noise associated with NF-κB immunofluorescence. p65-knockout cells stably expressing a p65-GFP fusion protein were exposed to a range of TNF concentrations, fixed, and immunostained for p65. The correlation between the direct and immunostained p65 measurements was used to estimate the amount of error that arises from immunostaining.

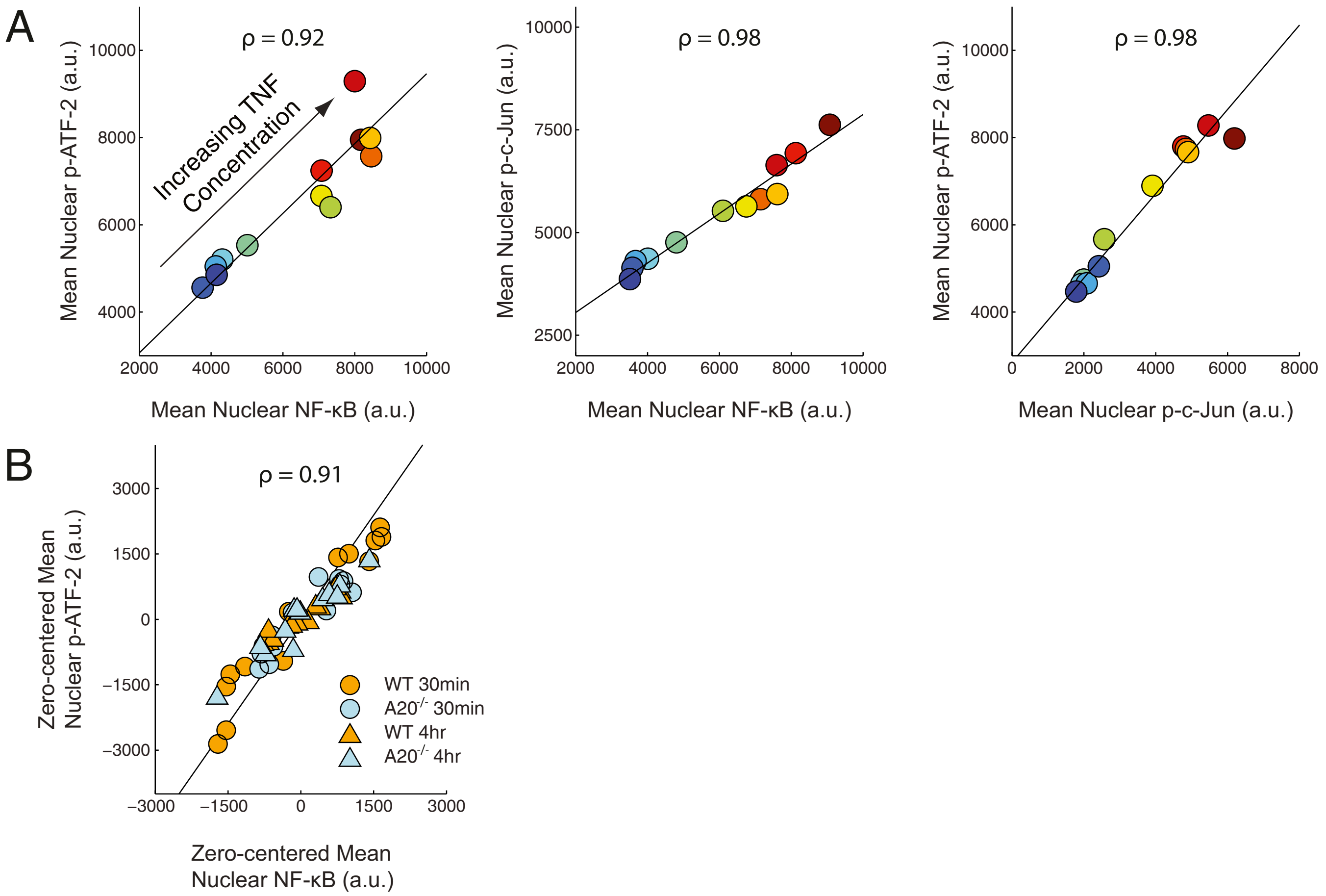

Fig. S3. Response pairs are linearly related. (*A*) Means of the data given in Fig. 3 *B–D* are shown. Each circle represents the mean response to a distinct concentration of TNF. The best-fit regression lines are shown and used as the basis for noise decomposition. (*B*) Data given in Fig. 5*B* were combined, centered about the origin, and plotted. The slope of the linear relationship between NF-κB and p-ATF-2 is the same at both the 30-min and 4-h time point for both wild-type and A20$^{-/-}$ cells.

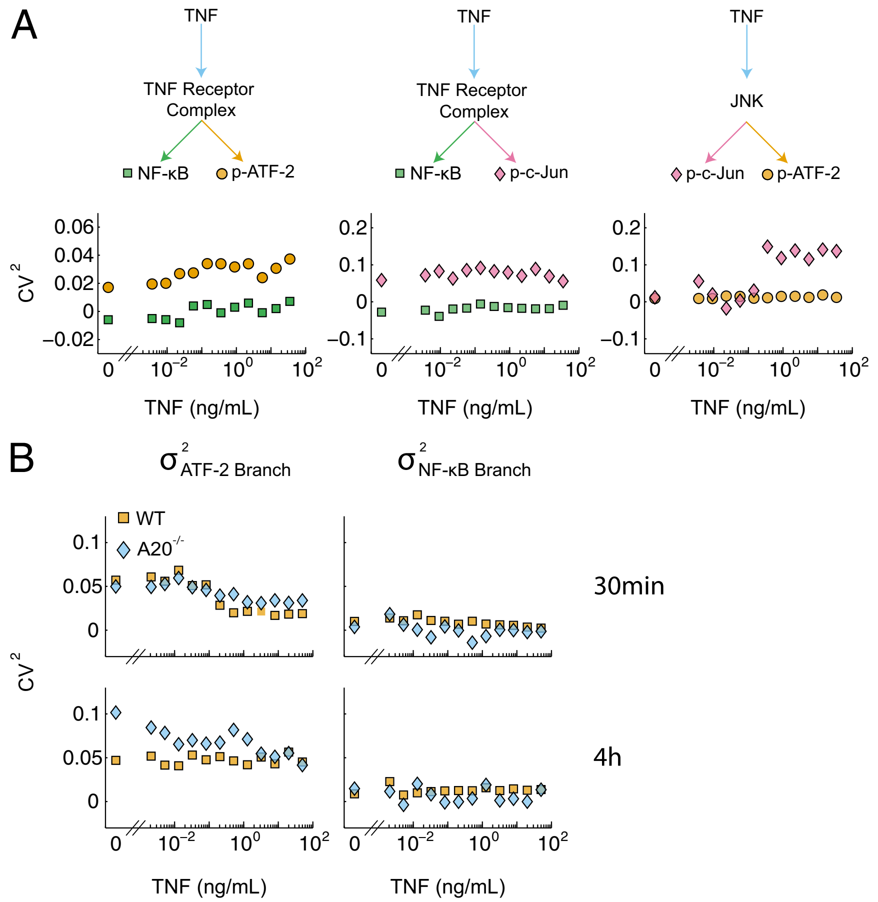

Fig. S4. Square of the coefficient of variation (CV^2) can elucidate underlying branch noise distributions. CV^2 is calculated for the data given in (*A*) Fig. 3 *B–D* and (*B*) Fig. 5*B*. Across TNF concentrations, branches, time points, and cell types, the CV^2 is relatively constant, which is suggestive of branch noise with log-normal or gamma distributions.

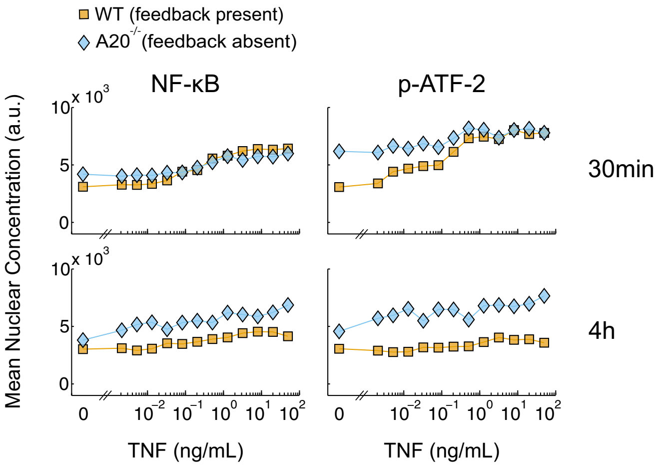

Fig. S5. Mean nuclear response of mutant and wild-type cells to TNF. The mean nuclear concentration of NF-κB and p-ATF-2 in response to TNF in both WT and A20$^{-/-}$ cells at 30 min and 4 h for the data shown in Fig. 5*B* in the main text.